

POSTULATED FAILURE ANALYSES OF TENSION LEG PLATFORM (TLP) RESTRAINING SYSTEM UNDER THE INFLUENCE OF VARYING SEA-STATE CONDITIONS

ANALIZA LOMA SISTEMA VEZE PREDNAPREGNUTE NOŽNE PLATFORME (TLP) POD UTICAJEM PROMENLJIVIH USLOVA NA MORU

Originalni naučni rad / Original scientific paper
UDK /UDC:

Rad primljen / Paper received: 6.04,2021

Adresa autora / Author's address:

¹) School of Petroleum Technology, Pandit Deendayal Petroleum University, Gujarat, India

²) Department of Ocean Engineering, Indian Institute of Technology, Madras, India

email: shanker.krishna@spt.pdpu.ac.in

Keywords

- offshore engineering
- Tension Leg Platform (TLP)
- tether
- Miner's rule
- rain-flow counting

Abstract

Increase in energy demand has led to an increase in hydrocarbon exploration and production in deep water environments. Tension Leg Platform (TLP) are taut moored floating type structures operational in deep-water environments. The restraining system, a taut moored tether, forms a critical component of the TLP. Tethers are held at a high pretension and subjected to continuous variation in stress due to the dynamic loads in the ocean environment. The dynamic loads due to continuous stress reversals cause fatigue. It is essential to analyse the fatigue life of such structures during the design phase. Tether pull-out can occur in the case of any undesirable loads acting on the restraining system. The study focuses on determining the fatigue life of the tether under normal operating conditions by employing rain-flow counting and Miner's rule. Also, fatigue life analysis is accomplished by considering the postulated failure condition in the restraining system, wherein one tether fails in each of the four legs. It is observed that there is a substantial reduction in fatigue life for the postulated failure condition. In the phenomenal sea-state condition, the fatigue life of tether reduces by 97% as compared to the normal operating condition.

INTRODUCTION

Offshore structures as TLP accomplish cost effectiveness in a deep-water operational environment, /1/. TLP are generally used at an operating water depth of 1000 to 5000 feet (300 to 1500 m), /2/. TLP's are position restrained by vertically taut moored tethers or tendons. These tethers are fastened to the seafloor by using templates. These templates are restrained by the use of piles that are driven into the seafloor, /3/. A schematic representation of the TLP is shown in Fig. 1. Tethers are tensioned and attached to the four corners of the hull which restricts the movement in heave, pitch and roll degrees of freedom (DOF) to a great extent. The pre-tension is imposed on the tethers by a de-ballasting procedure. TLP is compliant in the horizontal

Ključne reči

- ofšor inženjering
- prednapregnuta nožna platforma (TLP)
- veza
- Majnerovo pravilo
- prebrojavanje kišnog toka

Izvod

Povećane potrebe za energijom su dovele do porasta u istraživanju i proizvodnji ugljovodonika u dubokim vodenim sredinama. Prednapregnute nožne platforme (TLP) su čvrsto usidrene plutajuće konstrukcije u dubokim vodama. Sistem vezivanja, predstavljen čvrsto usidrenom vezom, je kritična komponenta TLP-a. Veze su pod velikim predopterećenjem i podvrgnute su stalnim promenama napona usled dinamičkih opterećenja u okeanskoj sredini. Dinamička opterećenja usled kontinuirane promene napona prouzrokuju zamor. Potrebno je analizirati životni vek zamora takvih konstrukcija tokom faze projektovanja. Popuštanje priveza može se dogoditi u slučaju neželjenih opterećenja koja deluju na sistem vezivanja. Ovaj rad se fokusira na određivanju veka zamora veze u normalnim radnim uslovima primenom prebrojavanja kišnog protoka i Majnerovog pravila. Takođe, zamorni vek se analizira razmatranjem pretpostavljenog stanja otkaza u sistemu za povezivanje, pri čemu otkazuje jedan vez na svakoj od četiri noge. Primećuje se značajno smanjenje veka zamora za pretpostavljeno stanje otkaza. U uslovima fenomena stanja mora, vek zamora veze se smanji za 97% u poređenju sa vekom zamora u normalnim radnim uslovima.

DOF i.e., surge, sway, and yaw, and restrained in the vertical DOF i.e., heave, roll, and pitch /4/.

The DOF for the movement of the platform are indicated in Fig. 2. The dynamic analyses of floating offshore structures being subjected to irregular waves is essential to determine the stress generated in the mooring systems. In floating systems, tethers play a major role in the service life of the platform and the fatigue analysis helps in the determination of it /2, 5/.

One of the initial analyses on a TLP was to determine the variability of the hydrodynamic load predictions. This was accomplished by carrying out the diffraction/radiation analyses in which the results from 17 organizations are plotted in a common format /8/. Several researches are carried out

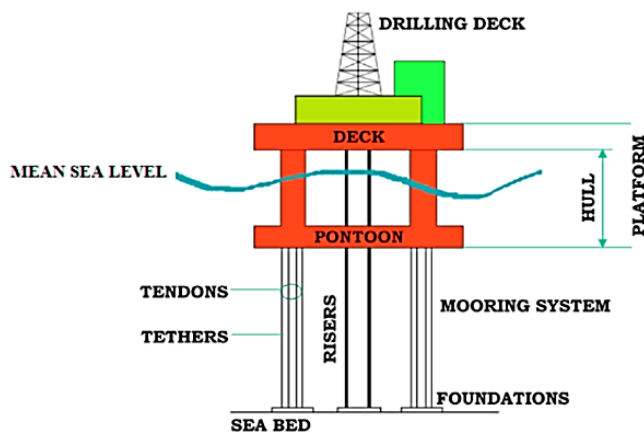


Figure 1. Schematic diagram of a TLP, /6/.

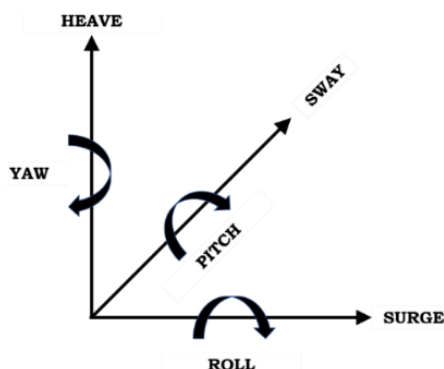


Figure 2. DOF in TLP motion, /7/.

further on TLPs for the hydrodynamic forces acting on the platform and its response behaviour. Dynamic analysis, both in frequency and time domain, is carried out wherein random waves act in arbitrary direction based on Pierson - Moskowitz spectrum /9/. Morison's equation, based on Airy's linear wave theory, is used to calculate the hydrodynamic forces. The responses, which are nonlinear in nature, are used to compute the displacements, velocities, and the accelerations. Numerical simulations in nonlinear time domain are carried out and the results are validated with experimental investigations on a scaled model, /10/. The TLP structure is subjected to wind and waves, and the platform motions and mooring tension are analysed. The results from the simulation are compared with experimental results and observed that the mooring tension values are in accordance with the numerical results, while some variations are observed in the dynamic equivalent fields. In order to determine the response of three different floating platforms, dynamic response investigations are conducted based on the environmental parameters of the South China sea /11/. The global and dynamic response analysis is carried out for a Spar platform, TLP, and semi-submersible platform. Hydrodynamic models employing the 3D potential theory are used for the study. Mathematical methods are used to investigate the TLP's hydrodynamic response, /12/. The hydrodynamic response is studied using a TLP model where the tensions in the tethers are measured using special load cells and motions in corresponding DOF are measured with accelerometers /13/. Numerical methods are used to determine the hydrodynamic response data, in order to

design TLP at Marmara Sea, /14/. Platforms with different drafts are compared in the study. It is observed that with a decrease in the platform's draft, there is an escalation in the surge response in the low frequency domain. The present study focuses on the fatigue life analysis of a TLP that is acted upon by waves and operates in various sea-states ranging from very rough to phenomenal. Further, a postulated failure analyses is also carried out by cutting one tether from each leg to observe the resulting reduction in fatigue life of the platform.

NUMERICAL MODELLING

Numerical modelling of the International Ship and Off-shore Structures Congress (ISSC) TLP is carried out using ANSYS® AQWA. ISSC TLP is composed of a hull mated to the deck. The hull is composed of four pontoons and four cylindrical columns forming a square geometry. The platform is modelled based on the structural details mentioned in Table 1. In order to simulate the fluid wave loading on the structure, radiation theory, or the three-dimensional diffraction theory is used. The predictor - corrector scheme is used in the dynamic simulation in time domain, in which a real-time simulation of a body that floats is carried out in each time-step by the integration of acceleration. TLP is modelled as shown in Fig. 4, based on the geometrical and structural details in Table 1.

Table 1. Structural details of the ISSC TLP, /15/.

Parameters	Dimensions
Diameter and spacing between centers of the column	86.25 m and 16.88 m
Pontoon height and width	7.50 m and 10.50 m
Draft at MWL	35.00 m
Displacement	5.346×10^5 kN
Platform weight	40.5×10^7 N
Total pretension in the tether	1.373×10^5 kN
Metacentric heights (longitudinal and transverse)	6.0 m each
Mass moment of inertia (roll)	82.37×10^9 kg-m ²
Mass moment of inertia (pitch)	82.37×10^9 kg-m ²
Mass moment of inertia (yaw)	98.07×10^9 kg-m ²
Vertical position of COG above keel	38.0 m
Mooring tether's length	415.0 m
Combined tethers' vertical stiffness (EA/L)	0.813×10^6 kN/m
Roll and pitch effective stiffness (EI _x /L and EI _y /L)	1.501×10^9 kN-m/rad

The pontoon connects the two columns together. The TLP consists of 12 tendons that are latched onto the foundation templates. There are 12 tendons that are attached to the hull of the platform near the keel. The geometry of the platform is shown in Fig. 3.

METHODOLOGY

The deck and hull of the TLP is modelled as a diffraction element in this dynamic analysis. The mass of the platform comprising of the deck and the hull is lumped at the centre of mass of the platform. Three-point Gaussian integration technique is used to calculate the hydrodynamic force. The platform obtains axial stiffness from tethers modelled as

cable elements. The initial pretension in the tethers is obtained by stretching of the tethers. A three-dimensional panel method is used for meshing the platform geometry. The equation of motion, as shown in Eq.(1), is solved in dynamic analysis with the help of convolution integration method,

$$[M+Ma]\ddot{x}(t)+[C]\dot{x}(t)+[K]x(t)=F(t), \quad (1)$$

where: displacement, velocity, acceleration and force vectors are denoted by $x(t)$, $\dot{x}(t)$ and $F(t)$, respectively. Structural mass matrix and added mass matrix are represented by $[M]$ and Ma , respectively. $[C]$ represents the damping matrix, while $[K]$ denotes the stiffness matrix. Dynamic analyses use Pierson-Moskowitz (PM) spectrum, /16/, which is a wave spectrum for a fully developed sea-state. Mathematical representation of the spectrum is shown in Eq.(2),

$$S^+(\omega)=\frac{1}{2\pi}\frac{H_s^2}{4\pi T_z^2}\left(\frac{2\pi}{\omega}\right)^5\exp\left(-\frac{1}{\pi T_z^4}\left(\frac{2\pi}{\omega}\right)^4\right), \quad (2)$$

where: $S^+(\omega)$ represents the wave spectrum; T_z denotes zero-crossing period; H_s represents significant wave height; and ω stands for frequency. Environmental parameters employed in this study are described in Table 2.

Table 2. Environmental conditions used for simulation, /5/.

Sea-states	Wave-heights (m)	Zero-crossing period (s)	Wind velocity (m/s)
S1	5.15	7.26	13.36
S2	8.15	9.14	16.81
S3	14.15	12.04	22.15
S4	17.15	13.26	24.38

Fatigue is a process by which accumulation of damage occurs in a material when subjected to stresses of fluctuating nature, /17, 18/. The loading process may not be large to cause a plastic deformation, or failure on immediate effect. The accumulated damage in the member reaches a critical level wherein the damage occurs. Due to the random waves, tethers, and mooring systems in offshore environments are subjected to fatigue damage and fatigue analysis forms an important criterion for the design aspects. Morison equation is used to determine the forces on the tethers due to the waves.

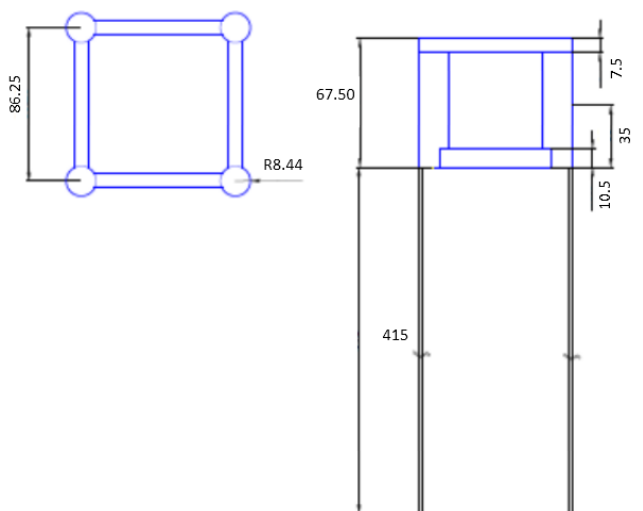


Figure 3. The geometry of TLP model /1/ (all dimensions in m).

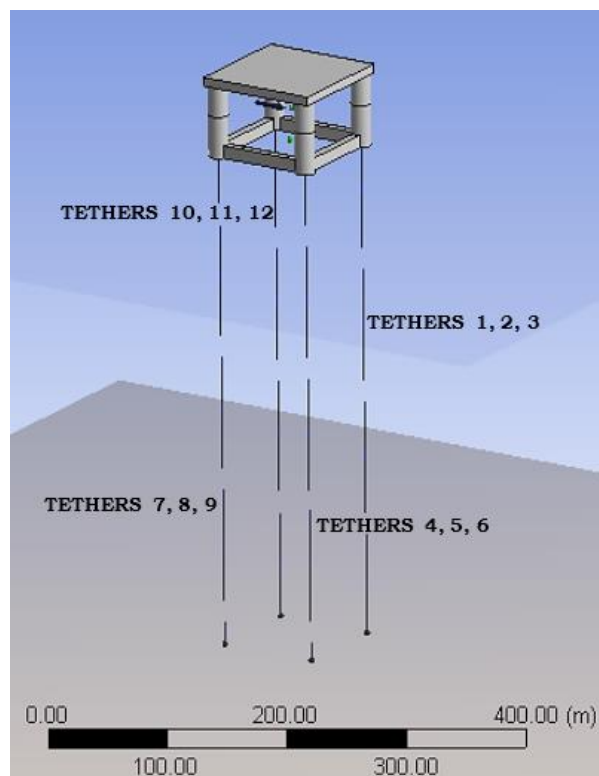


Figure 4. Numerical model of ISSC TLP.

RAIN-FLOW COUNTING AND MINER'S RULE

Variable submergence of the hull during the wave load action causes the pre-tension in the tethers to vary with time. The platform is being subjected to random wave action and the variation of stress in the tethers shall also be random and largely depends on the offset and set-down motion of the tension leg platform. The cycle average and range for a broad band spectrum can be determined using rain-flow counting. The pre-tension in the tethers make the stress response of the tether to be a non-zero mean process.

Therefore, once the cycle range and averages are obtained, Goodman diagram is used to convert each cycle to a stress range having zero mean. S-N curves are used to compute the number of cycles that are necessary for a fatigue failure to occur. In the bilinear curve, the slope m is 3, $\log_{10}a$ is 12.081 which is the intercept in the $\log N$ axis which is applicable up to 10^3 MPa beyond which the slope changes to $m = 5$ and $\log_{10}a$ is 16.081. The endurance limit at 10^8 cycles is 41.45 N/mm^2 , /19/.

Fatigue analysis is carried out by S-N technique which employs cumulative damage models which relate stress to life. In the S-N technique the cumulative damage due to fatigue is taken into consideration wherein failure occurs after N loading cycles for a given stress range (S). The relationship between loading cycles and stress range is represented by Eq.(3),

$$\log N = \log A - m \log S, \quad (3)$$

where: constants A and m are determined experimentally from the S-N curve of the material being subjected to the fatigue analysis; N represents the number of permissible cycles; and S denotes the stress range. This technique is often used to determine service life of the platform. The stress-

time history and the variation in the tether tension is obtained by dynamic analysis. The range of stress and number of cycles is obtained from the stress histogram using the rain-flow counting technique.

The calculation of the permissible number of cycles is based on DNV-RP-C203 code /19/. Miner’s rule is used for computation of fatigue damage accumulation in cumulative damage models. According to Miner’s rule, failure due to fatigue occurs when strain energy of ‘*n*’ variable amplitude cycles equals ‘*N*’ cycles with constant amplitude. The mathematical representation of Miner’s rule is shown in Eq.(4),

$$D = \sum_{i=1}^m \frac{n_i}{N_i} \tag{4}$$

The histogram provides the value of the number of counts, represented by *n*. The count of permissible cycles is represented by *N* and it is derived from S-N curves. *D* represents the fatigue damage. The capability to perform the intended function within in the design life of a member is termed to be reliable. Reliability index (*β*), an indicator of the probability of failure, is shown in Eq.(5),

$$\beta = \frac{\mu_R - \mu_S}{\sqrt{\sigma_R^2 + \sigma_S^2}} \tag{5}$$

where: μ_R is the mean resistance 630.8 N/mm²; σ_R standard deviation of resistance is 33.7 N/mm². The mean demand is represented by μ_S (in N/mm²); and the respective standard deviations are denoted by σ_S (in N/mm²), /20/. The chance of failure due to yielding of the tether is given by probability of failure which is determined from the cumulative distribution function of standard normal distribution as shown in Eq.(6),

$$P_f = \phi^{-1}(-\beta) \tag{6}$$

where: reliability index and normal cumulative distribution function are represented by ϕ and β , respectively.

RESULTS AND DISCUSSION

Failure of a tether under each leg has caused a reduction in the stiffness of the overall restraining system. The effect resulting from the postulated failure on the tethers is shown in Table 3. There is a reduction of 33.33 % in the stiffness of the tethers.

This reduction in the stiffness of the restraining system has caused an increase in pre-tension in the tether by 49.29 % to compensate for the reduction. The comparison of stiffness of the restraining system and the pretension per tether under normal operation and postulated failure conditions is shown in Table 3.

Table 3. Environmental conditions used for the simulation.

Properties	Normal operating conditions	After failure of 4 tethers
Stiffness of the restraining system in MN/m	657.628	438.419
Pretension per tether (MN)	10.580 - 10.581	15.795 - 15.810

Dynamic analysis is initially carried out with all the 12 tethers under the sea-states given in Table 2. In sea-state S4 (phenomenal), the maximum variation in the tension from the initial pretension is found to be 2.61 MN, which is

about 24.73 % of initial pre-tension. The maximum value of stress developed is found to be 111.019 MPa, which is about 82.40 % of the yield stress of steel.

The postulated failure conditions with 4 tethers failed (one in each of the four legs of the platform) is studied under similar operating conditions as shown in Table 2. In sea-state S4 (phenomenal), the maximum variation in the tension is found to be 4.76 MN, which is about 30.16 % of initial pre-tension. The maximum value of stress developed is found to be 190.035 MPa, which is about 69.87 % of the yield stress of steel.

The stress variations caused in normal operating conditions of TLP and in postulated failure condition are shown in Figs. 5 to 8 for the four sea-states shown in Table 2. Summary of the descriptive statistics of 6th tether under normal operation and postulated failure conditions is shown in Tables 4 and 5 for the four sea-states shown in Table 2.

Zero skewness implies that distribution of the stress is symmetric about the mean stress value. Since Mean, Median and Mode are same in all cases, and Kurtosis is near to 3, the distribution followed by the stress process is considered as a normal/Gaussian distribution which confirms the application of reliability concepts.

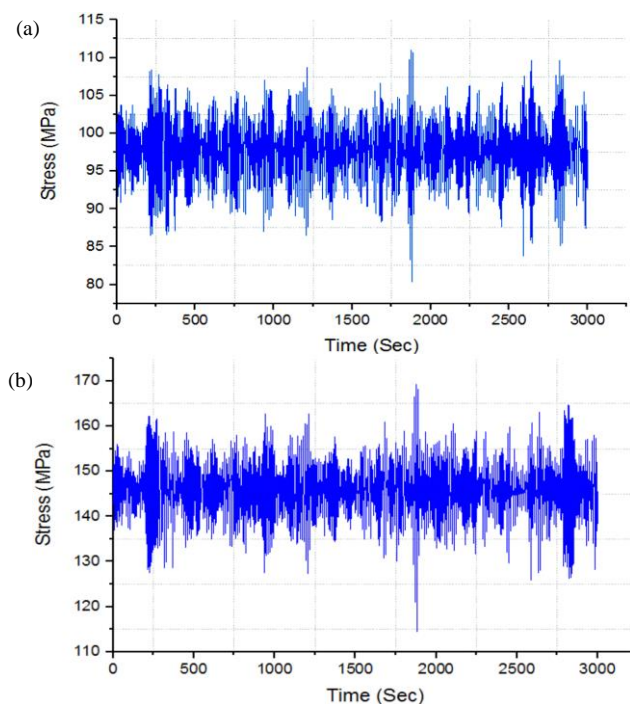
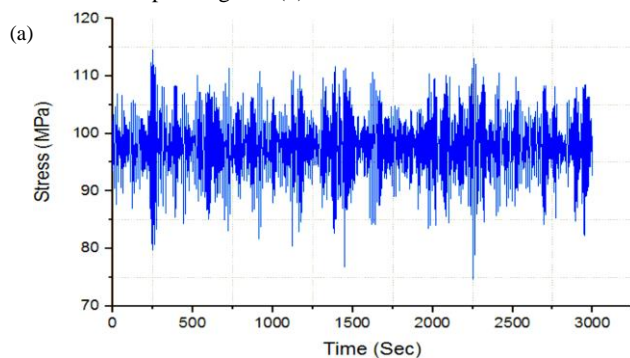


Figure 5. Variation in stress for sea-state S1 under (a) normal operating and (b) tether-cut condition.



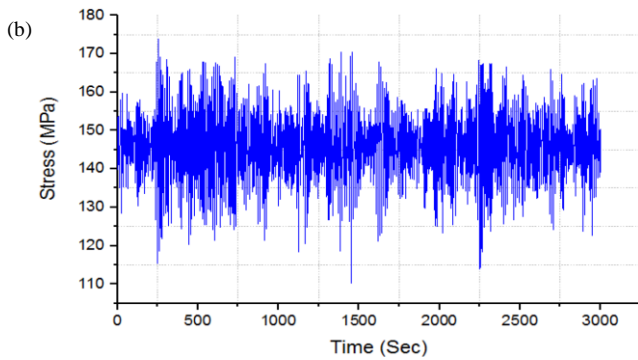


Figure 6. Variation in stress for sea-state S2 under (a) normal operating and (b) tether-cut condition.

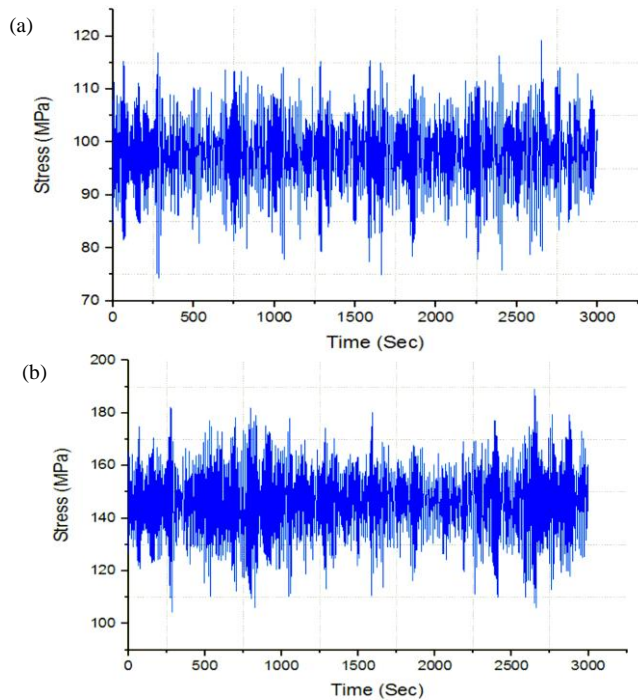


Figure 7. Variation in stress for sea-state S3 under (a) normal operating and (b) tether-cut condition.

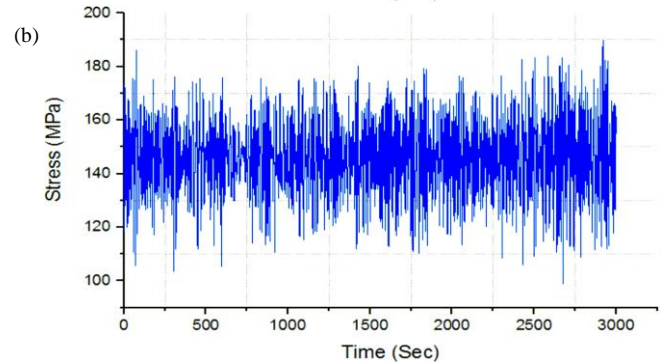
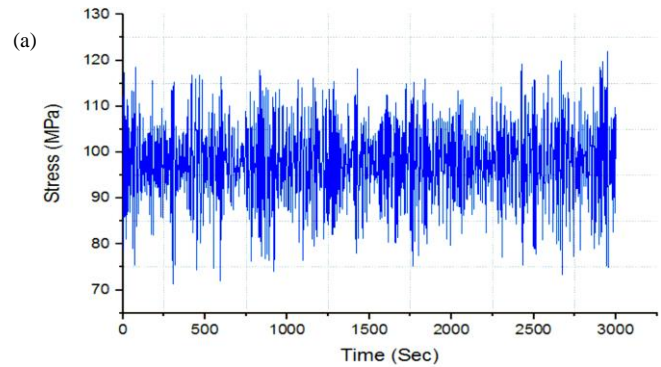


Figure 8. Variation in stress for sea-state S4 under (a) normal operating and (b) tether-cut condition.

The value of reliability index (β) for normal operating conditions ranges from 15.720 to 15.416, therefore, probability of failure for normal operating conditions ranges from $5.5162e^{-56}$ to $6.3889e^{-54}$. In the postulated failure case, the value of reliability index (β) varies from 14.174 to 13.455, therefore, the probability of failure ranges from $6.6360e^{-46}$ to $1.4387e^{-41}$.

Figures 9 to 12 represent the rain-flow counting matrices of 6th tether for the four sea-state conditions given in Table 2. For sea-states S1 to S4, in normal operating condition the mean stress varies from 97.672 to 97.749 N/mm² and the maximum stress cycle range varies from 30 to 50 N/mm².

Table 4. Summary of descriptive statistics for 6th tether.

Sea-state	Mean (μ_S)	Median (\tilde{x})	Mode	σ_S	Skewness	Kurtosis (K_4)	Reliability index (β)
S1	97.702	97.879	98.326	3.783	-0.194	3.260	15.720
S2	97.672	97.840	97.820	5.258	-0.202	3.157	15.630
S3	97.749	98.034	99.202	6.442	-0.198	2.992	15.536
S4	97.717	97.937	97.937	7.749	-0.168	2.903	15.416

Table 5. Summary of descriptive statistics for 6th tether in tether-cut condition.

Sea-state	Mean (μ_S)	Median (\tilde{x})	Mode	σ_S	Skewness	Kurtosis (K_4)	Reliability index (β)
S1	145.872	146.078	144.794	5.895	-0.183	3.358	14.174
S2	145.851	146.020	143.976	8.405	-0.176	3.161	13.962
S3	145.982	146.293	141.465	11.056	-0.132	3.078	13.669
S4	145.995	146.195	142.321	12.744	-0.111	2.904	13.455

For the postulated failure condition, the rain-flow counting matrices corresponding to the 6th tether for the four sea-states given in Table 2 are shown in Figs. 13 to 16. For sea-states S1 to S4, in postulated failure condition, the mean stress varies from 145.851 to 145.995 N/mm² and the maximal stress cycle range varies from 60 to 100 N/mm².

An increase in stress fluctuations is observed in the postulated failure condition as compared with that in normal operating condition. The observations from Figs. 9 to 12 for the

normal operating conditions of the TLP are shown in Table 6, while observations from Figs. 13 to 16 for the postulated failure conditions are given in Table 7.

A comparison of fatigue life of the 6th tether under four sea-states in normal operation and in postulated failure conditions is shown in Table 8. Under normal conditions the prestress is about 97 N/mm². Most of the cycles are concentrated at an average of 97, as can be observed from Figs. 9-12.

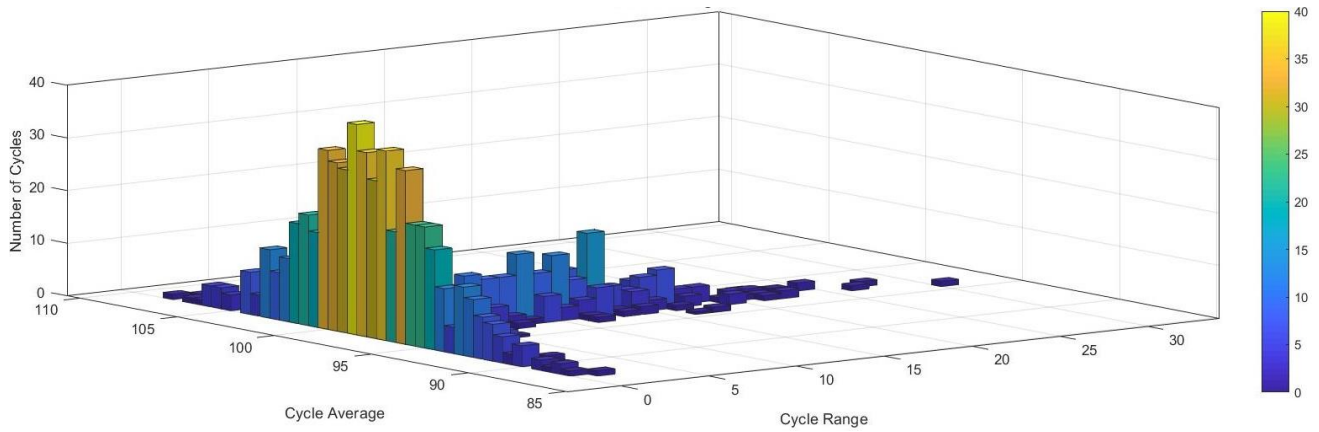


Figure 9. Rain-flow counting matrix for 6th tether under sea-state S1,

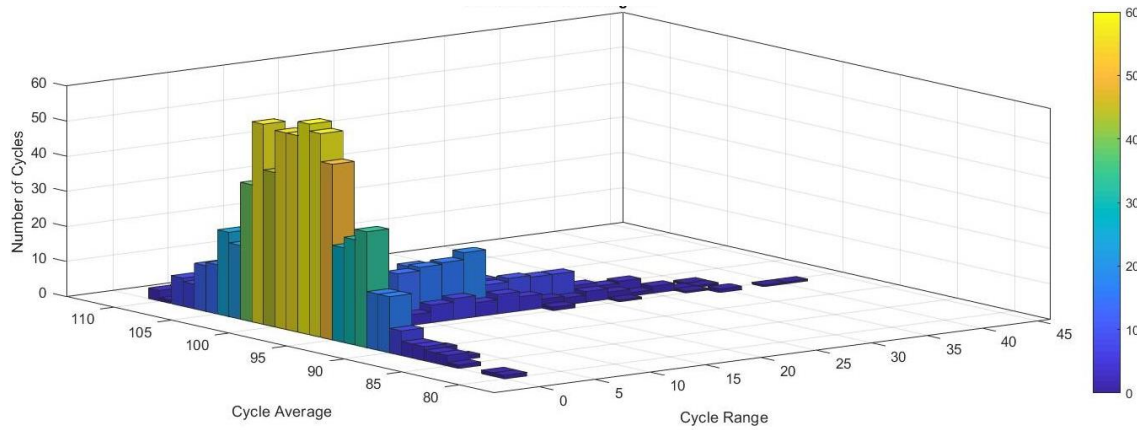


Figure 10. Rain-flow counting matrix for 6th tether under sea-state S2.

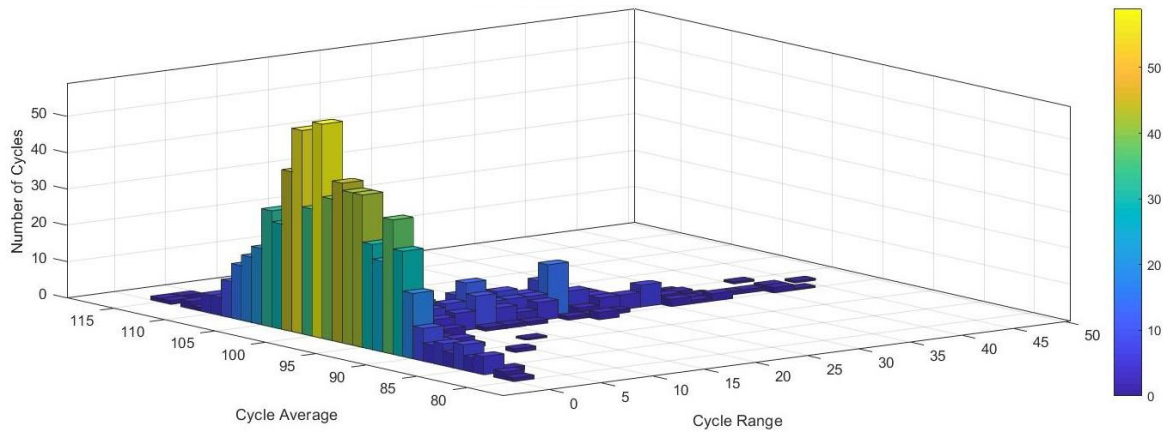


Figure 11. Rain-flow counting matrix for 6th tether under sea-state S3.

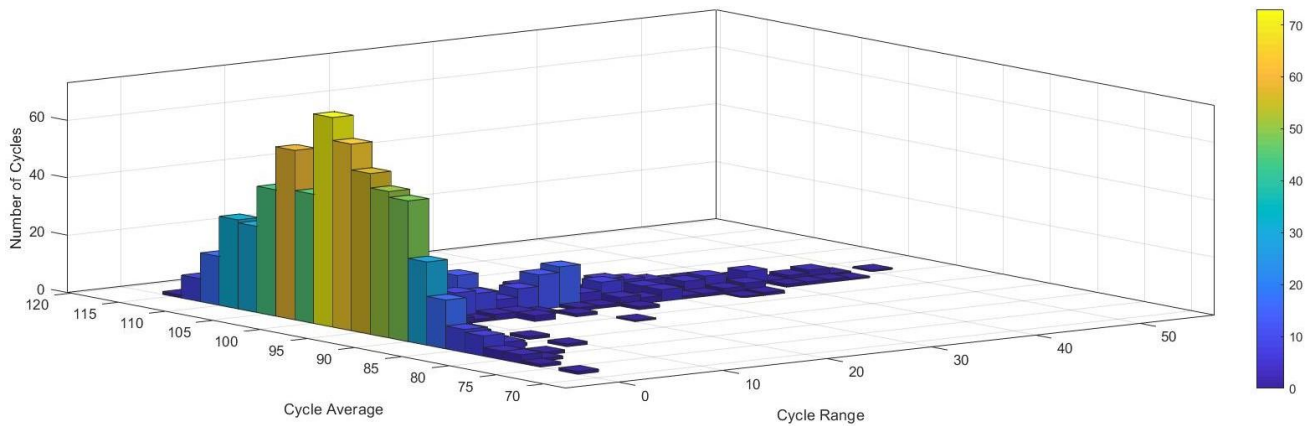


Figure 12. Rain-flow counting matrix for 6th tether under sea-state S4.

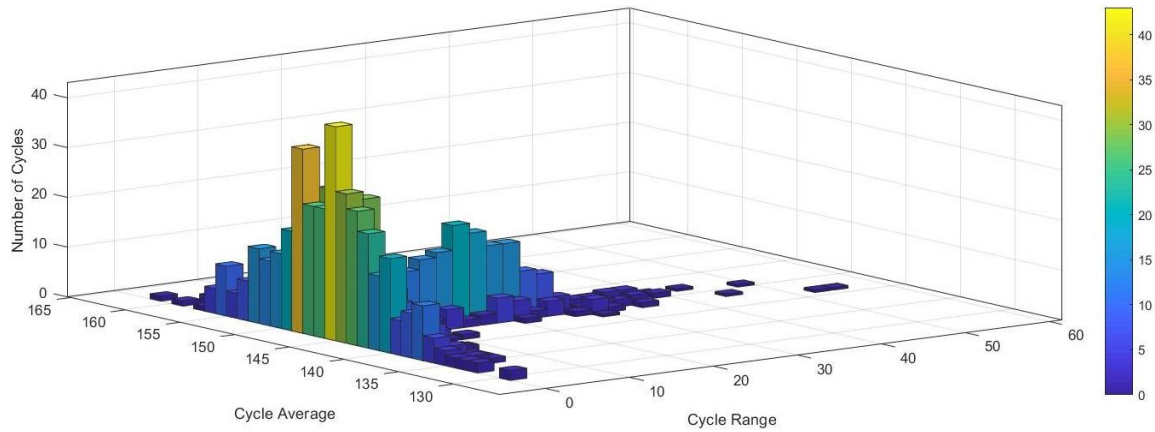


Figure 13. Rain-flow counting matrix for 6th tether under sea-state S1 in postulated failure condition.

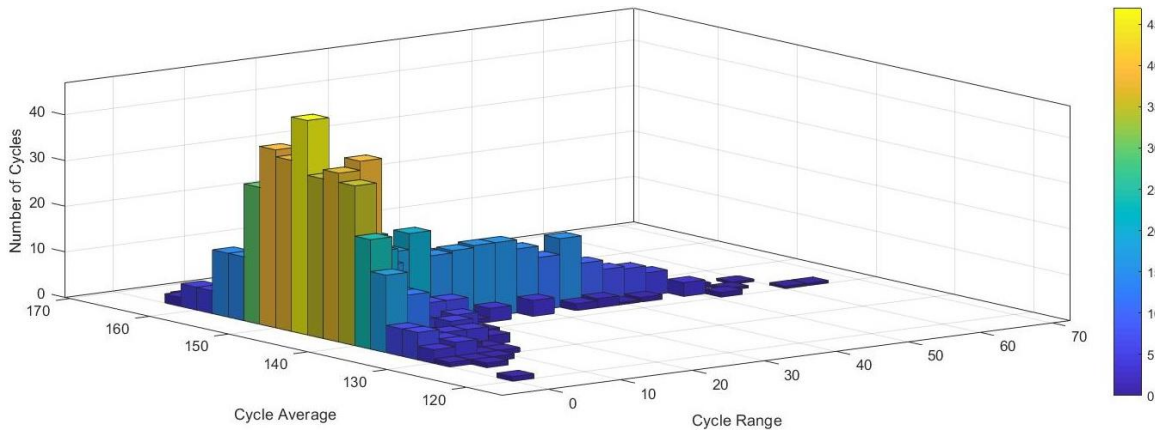


Figure 14. Rain-flow counting matrix for 6th tether under sea-state S2 in postulated failure condition.

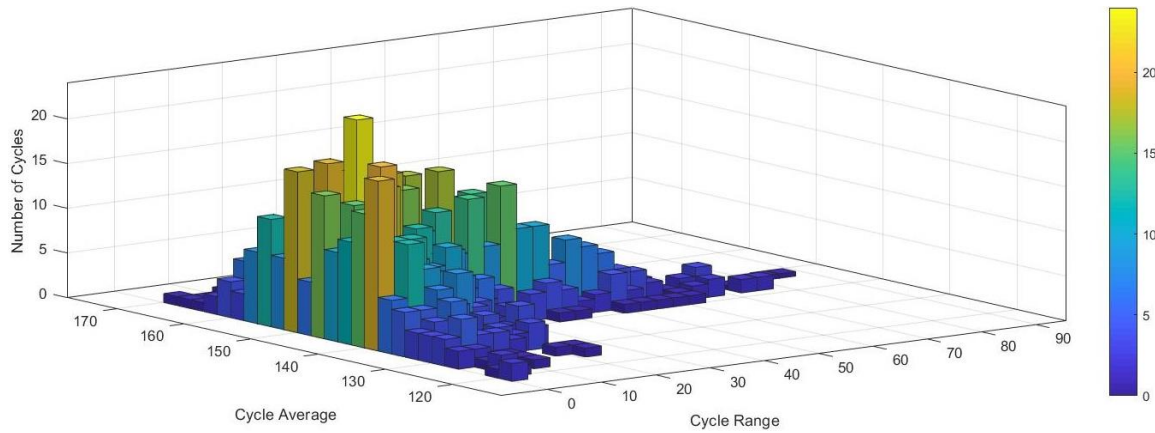


Figure 15. Rain-flow counting matrix for 6th tether under sea-state S3 in postulated failure condition.

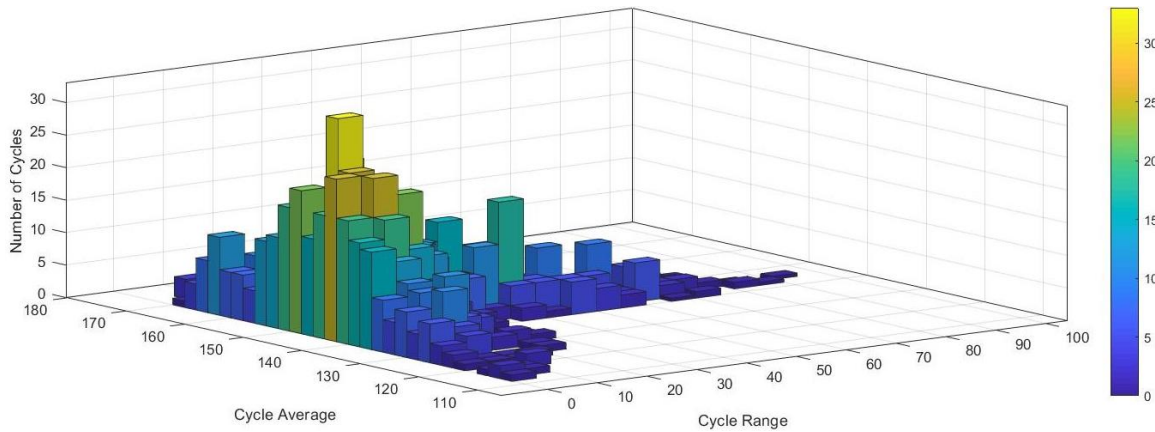


Figure 16. Rain-flow counting matrix for 6th tether under sea-state S4 in postulated failure condition.

Table 6. Observations from rain-flow counting matrix for 6th tether under normal operation.

Sea-state	Maximal stress cycle range (N/mm ²)	Mean stress (N/mm ²)	Var. in stress cycle range (N/mm ²)	Variation in cycle average (N/mm ²)
S1	30	97.7	0-30	85-110
S2	45	97.672	0-45	80-110
S3	50	97.749	0-50	80-115
S4	50	97.717	0-50	70-115

Table 7. Observations from rain-flow counting matrix for 6th tether under tether-cut condition.

Sea-state	Maximal stress cycle range (N/mm ²)	Mean stress (N/mm ²)	Var. in stress cycle range (N/mm ²)	Variation in cycle average (N/mm ²)
S1	60	145.872	130-165	0-60
S2	70	145.851	120-170	0-70
S3	90	145.982	120-170	0-90
S4	100	145.995	110-180	0-100

Table 8. Fatigue life of 6th tether in 4 different sea-states S1 to S4.

Sea-state	Fatigue life in normal operating conditions (years)	Fatigue life in postulate failure conditions (years)
S1	Negligible damage in accordance with Miner's rule	700.952
S2	Negligible damage in accordance with Miner's rule	56.712
S3	2910	8.891
S4	246.427	5.127

In postulated failure conditions the stress in the tether has increased to 145 N/mm² and also most of the cycles are surrounded with a cycle average of 145 N/mm² as observed in Figs. 13-16. This describes pre-stress shifting from 95 to 145 N/mm² and the tether is undergoing stress variation about the shifted position. Also, after failure, cycle ranges are more and frequent which results in more damage in the material ultimately leading to failure in lesser time. The same has been observed in the results.

CONCLUSIONS

In this investigation, the dynamic analysis is conducted for a TLP using the Pierson Moskowitz spectrum for four different sea states with increasing wave heights. Fatigue life analysis is carried out on tethers of the TLP, for both normal operating conditions as well as for postulated failure conditions. The following prominent observations are noted:

- statistical analysis of the tether response stress reversals shows that the distribution is approximately symmetric from the skewness values. Also, it is observed that the distribution follows a Gaussian distribution from the Kurtosis, mean, median and mode values;
- the reliability index (β), that shows the safety level of the system reduces during the postulated failure condition;
- in the dynamic analysis carried out in the phenomenal sea state, under normal operating condition of TLP, i.e. with all 12 tethers, an increase in the tether tension up to 24.73 % of initial pre-tension is seen. The stress observed have not consumed 82.4% of the yield stress of steel;
- in the dynamic analysis carried out in the phenomenal sea state, under postulated failure condition of TLP, i.e. with

8 tethers, an increase in tether tension up to 30.16 % of initial pre-tension is seen. The stress observed is close to 69.87 % of the yield stress of steel;

- the fatigue life in the phenomenal sea state for normal operating condition of TLP is 246.52 years while for the postulated failure 5.127 years. This decrease in fatigue life is caused due to the increased pre-tension and stress due to the reduction in stiffness of the tether. A fatigue life reduction is higher when the sea state increases from very-rough to phenomenal condition.

REFERENCES

1. Fang, H., Duan, M., Offshore Operation Facilities: Equipment and Procedures, Gulf Professional Publishing, 2014.
2. Ma, K.T., Luo, Y., Kwan, C.T.T., Wu, Y., Mooring System Engineering for Offshore Structures, Gulf Professional Publishing, 2019.
3. Speight, J.G., Handbook of Offshore Oil and Gas Operations, Gulf Professional Publishing, 2014.
4. Chakrabarti, S.K. (Ed.), Handbook of Offshore Engineering (2-Vol. set), Elsevier, 2005.
5. Siddiqui, N.A., Ahmad, S. (2001), *Fatigue and fracture reliability of TLP tethers under random loading*, Marine Struct. 14 (3): 331-352. doi: 10.1016/S0951-8339(01)00005-3
6. Taylor, R.E., Jefferys, E.R. (1986), *Variability of hydrodynamic load predictions for a tension leg platform*, Ocean Eng. 13(5): 449-490. doi: 10.1016/0029-8018(86)90033-8
7. Tabeshpour, M.R., Hedayatpour, R. (2019), *Analytical investigation of nonlinear heave-coupled response of tension leg platform*, Proc. Inst. Mech. Eng., Part M: J Eng. Maritime Environ. 233(3): 699-713. doi: 10.1177/1475090218776430
8. Reza, A., Sedighi, H.M. (2015), *Nonlinear vertical vibration of tension leg platforms with homotopy analysis method*, Adv. Appl. Math. Mech. 7(3): 357-368. doi: 10.4208/aamm.2013.m314
9. Tabeshpour, M.R., Golafshani, A.A., Seif, M.S. (2006), *Comprehensive study on the results of tension leg platform responses in random sea*, J Zhejiang Univ. - Sci. A, 7(8): 1305-1317. doi: 10.1631/jzus.2006.A1305
10. Zhu, H., Ou, J. (2011), *Dynamic performance of a semi-submersible platform subject to wind and waves*, J Ocean Univ. China, 10(2): 127-134. doi: 10.1007/s11802-011-1755-z
11. Li, B., Liu, K., Yan, G., Ou, J. (2011), *Hydrodynamic comparison of a semi-submersible, TLP, and Spar: Numerical study in the South China Sea environment*, J Marine Sci. Appl. 10(3): 306. doi: 10.1007/s11804-011-1073-2
12. Gu, J.Y., Yang, J.M., Lv, H.N. (2012), *Studies of TLP dynamic response under wind, waves and current*, China Ocean Eng. 26(3): 363-378. doi: 10.1007/s13344-012-0028-y
13. Kurian, V.J., Idichandy, V.G., Ganapathy, C. (1993), *Hydrodynamic response of tension-leg platforms - A model*, Exp. Mech. 33(3): 212-217. doi: 10.1007/BF02322576
14. Söylemez, M., Yılmaz, O. (2003), *Hydrodynamic design of a TLP type offloading platform*, Ocean Eng. 30(10): 1269-1282. doi: 10.1016/S0029-8018(02)00107-5
15. Senjanović, I., Tomić, M., Hadžić, N. (2013), *Formulation of consistent nonlinear restoring stiffness for dynamic analysis of tension leg platform and its influence on response*, Marine Struct. 30: 1-32. doi: 10.1016/j.marstruc.2012.10.007
16. Pierson Jr, W.J., Moskowitz, L. (1964), *A proposed spectral form for fully developed wind seas based on the similarity theory of SA Kitaigorodskii*, J Geophys. Res. 69(24): 5181-5190. doi: 10.1029/JZ069i024p05181
17. Almar-Naess, A., Haagen, P.J., Lian, B., et al. (1984), *Investigation of the Alexander L. Kielland failure - metallurgical and*

- fracture analysis*, J Energy Resour. Technol. 106(1): 24-31. doi: 10.1115/1.3231014
18. Naess, A., Moan, T., Stochastic Dynamics of Marine Structures, Cambridge University Press, 2013. doi: 10.1017/CBO9781139021364
19. DNVGL-RP-C203: Fatigue design of offshore steel structures, Det Norske Veritas, 2011.
20. Sadowski, A.J., Rotter, J.M., Reinke, T., Ummenhofer, T. (2015), *Statistical analysis of the material properties of selected structural carbon steels*, Struct. Safety, 53(C): 26-35. doi: 10.1016/j.strusafe.2014.12.002

© 2021 The Author. Structural Integrity and Life, Published by DIVK (The Society for Structural Integrity and Life 'Prof. Dr Stojan Sedmak') (<http://divk.inovacionicentar.rs/ivk/home.html>). This is an open access article distributed under the terms and conditions of the [Creative Commons Attribution-NonCommercial-NoDerivatives 4.0 International License](#)

ECF23, European Conference on Fracture 2022

June 27 – July 1, 2022. Funchal, Madeira, Portugal

Fracture Mechanics and Structural Integrity

Sponsored by ESIS – European Structural Integrity Society



Unfortunately, the Corona virus pandemic problem has evolved to a situation that makes the realization of ECF23, on its present schedule, not possible. New deadline for ESIS Support for Researchers: March 31st, 2022

Dear Colleagues,

On behalf of the European Structural Integrity Society (ESIS) we have the pleasure to extend a warm welcome to all researchers planning to attend the 23rd European Conference on Fracture – ECF23, scheduled from June 27-July 1, 2022, on the beautiful Madeira Island, Portugal.

A Summer School on 25-26 June 2022, will take place as part of the conference. The two days event is mainly aimed at PhD students, young researchers and engineers, but it is open to everybody.

The conference will be held on one of the most emblematic hotels in Funchal, authored by the genius of Oscar Niemeyer, the Casino Park Hotel. The huge offer of hotels in Funchal provides the necessary conditions for every sort of visitors, constituting an invaluable argument for the organisation of a large conference such as ECF.

ECF23 focus will be twofold, on dynamical aspects of Structural Integrity and the largely unobserved realm of Integrity loss under dynamical loads as well as the developments of the monitoring technical aspects and their pitfalls as dynamics particularities take precedence over the phenomena we have come to know so well.

Aim and Topics

The conference topics include but are not limited to: Additive Manufacturing; Adhesives; Analytical, computational and physical models; Artificial Intelligence, Machine Learning and Digitalization in Fracture and Fatigue; Biomechanics; Ceramics; Composites; Computational Mechanics; Concrete & Rocks; Corrosion; Creep; Damage Mechanics; Durability; Environmentally Assisted Fracture; Experimental Mechanics; Failure Analysis and Case Studies; Fatigue; Fatigue Crack Growth; Fractography and Advanced metallography; Fracture and fatigue testing systems; Fracture and fatigue of additively manufactured materials or structures; Fracture and fatigue problems in regenerative energy systems (wind turbines, solar cells, fuel cells, ...); Fracture under Mixed-Mode and Multiaxial Loading; Functional Graded Materials; Hydrogen embrittlement; Image analysis techniques Impact & Dynamics; Innovative Alloys; Joints and Coatings; Linear and Nonlinear Fracture Mechanics; Mesomechanics of Fracture; Micromechanisms of Fracture and Fatigue; Multi-physics and multi-scale modelling of cracking in heterogeneous materials; Nanomaterials; Non-destructive inspection; Polymers; Probabilistic Fracture Mechanics; Reliability and Life Extension of Components; Repair and retrofitting; modelling and practical applications; Smart Materials; Structural Integrity; Temperature Effects; Thin Films

Conference Chairmen

Pedro M. G. P. Moreira, Phone: +351 22 041 4902

Luís Reis, IST, Phone: +351 96 641 5585

Email : ecf23@ecf23.eu

Important deadlines

Abstract submission, please submit your work by email to ecf23@ecf23.eu by February 28, 2022

Abstract acceptance notification by March 05, 2022

Full paper submission (Procedia) by August 20, 2022

Authors are invited to submit a maximum of two one-page abstracts (in English). All abstracts will be peer-reviewed based on originality, technical quality and presentation. The abstract should be prepared according to the template, which can be downloaded from http://ecf23.eu/abstract_ECF23.docx and submitted by email to ecf23@ecf23.eu

When submitting an abstract for a particular symposium please indicate so in your email.

Publication in Elsevier Journal

Authors are encouraged to submit a full conference paper of 6-8 pages. Reviewed and accepted conference papers will be published in a dedicated issue in Elsevier's Procedia Structural Integrity and made available in open-access at <http://www.journals.elsevier.com/procedia-structural-integrity/> after the conference.

Your paper should be submitted by August 20, 2022, at the latest. Please note that your full manuscript should abide by the full paper template and follow the paper preparation guidelines, which are available at http://ecf23.eu/PROSTR_ECF23_Template.docm Full paper template: [Word template](#) , [Latex and Word template](#) (zip file)

Important: Getting your abstract accepted does not mean that you are registered for the conference. Remember to register and pay for the conference before April 15th, 2022, in order to get a discount on the participation fee. You can also book your accommodation and social arrangements through the conference registration.